THE JOURNAL OF PHYSICAL CHEMISTRY Letters

pubs.acs.org/JPCL Letter

Predictive First-Principles Modeling of a Photosynthetic Antenna Protein: The Fenna–Matthews–Olson Complex

Yongbin Kim, Dmitry Morozov, Valentyn Stadnytskyi, Sergei Savikhin, and Lyudmila V. Slipchenko*

Cite This: J. Phys. Chem. Lett. 2020, 11, 1636–1643 Read Online

ACCESS | Metrics & More | Article Recommendations | Supporting Information

ABSTRACT: High efficiency of light harvesting in photosynthetic pigment–protein complexes is governed by evolutionary-perfected protein-assisted tuning of individual pigment properties and interpigment interactions. Due to the large number of spectrally overlapping pigments in a typical photosynthetic complex, experimental methods often fail to unambiguously identify individual chromophore properties. Here, we report a first-principles-based modeling protocol capable of predicting properties of pigments in protein environment to a high precision. The technique was applied to successfully uncover electronic properties of the Fenna–Matthews–Olson (FMO) pigment–protein complex. Each of the three subunits of the FMO complex contains eight strongly coupled bacteriochlorophyll *a* (BChl *a*) pigments. The excitonic structure of FMO can be described by an electronic Hamiltonian containing excitation (site) energies of BChl *a* pigments and electronic couplings between them. Several such Hamiltonians have been developed in the past based on the information from various spectroscopic measurements of FMO; however, fine details of the excitonic structure and energy transfer in FMO, especially assignments of short-lived high-energy sites, remain elusive. Utilizing polarizable embedding quantum mechanics/molecular mechanics with the effective fragment potentials, we computed the electronic Hamiltonian of FMO that is in general agreement with previously reported empirical Hamiltonians and quantitatively reproduces experimental absorption and circular dichroism spectra of the FMO protein. The developed computational protocol is sufficiently simple and can be utilized for predictive modeling of other wild-type and mutated photosynthetic pigment–protein complexes.

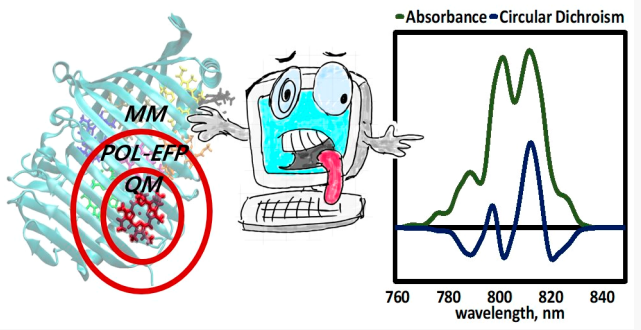

Plants, algae, and photosynthetic bacteria capture solar radiation by means of pigment–protein antenna complexes. A variety of natural antenna complexes evolved to maximize photosynthetic efficiency in different environments. The light harvesting and energy transfer efficiency of these complexes approaches 100% and is governed by electronic properties of individual light-absorbing pigments as well as by couplings between the pigments. While molecular structures of many antenna complexes have been determined by X-ray diffraction, the information about electronic energy levels and energy transfer dynamics often lacks desired precision as it is primarily deduced from optical data. Most of the antenna complexes contain large number of pigments (up to ∼250 000 in chlorosome antenna[1]) with overlapping optical spectra, leading to spectral congestion that precludes unambiguous identification of properties of individual pigments and, as a result, multiple models can be proposed to fit the same data. Fenna–Matthews–Olson (FMO) pigment–protein complex, found in green sulfur bacteria, is one of the most thoroughly studied photosynthetic proteins (see Figure 1).[2−37] The primary function of FMO is to transfer the excitation energy from a much larger chlorosome antenna to the intramembrane reaction center complex, where electronic excitation initiates charge transfer process.

The FMO complex is a trimer possessing C_3 symmetry. Each subunit encloses seven bacteriochlorophyll *a* (BChl *a*) chromophores and binds the eighth BChl *a* pigment between the subunits. Close packing of BChl *a* pigments in each monomer subunit leads to strong excitonic interactions and delocalization of excited states over multiple pigments. A relative structural simplicity combined with intricate excitonic structure makes the FMO complex a favorite object for developing and testing new computational and experimental techniques. For example, FMO was the first pigment–protein complex for which quantum coherences and beatings between excitonic states were observed by Savikhin et al. in 1997.[38] The study of excitonic structure and coherence in this complex led later to the development of a two-dimensional spectroscopy.[8,39−41] To model excitonic interactions and energy transfer

Received: November 25, 2019
Accepted: February 4, 2020
Published: February 4, 2020

https://dx.doi.org/10.1021/acs.jpclett.9b03486
J. Phys. Chem. Lett. 2020, 11, 1636–1643

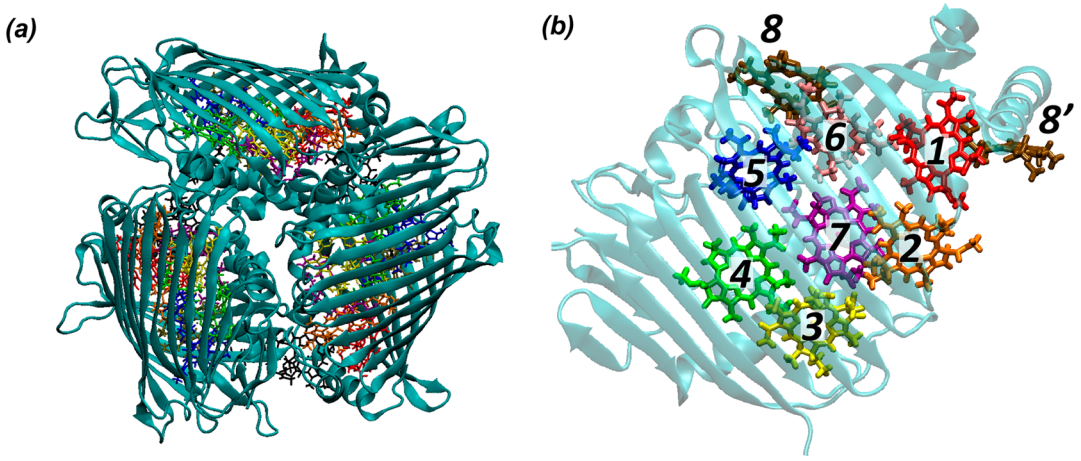

Figure 1. (a) FMO trimer of the *Chlorobaculum tepidum*; (b) FMO monomer with BChl *a* pigments.

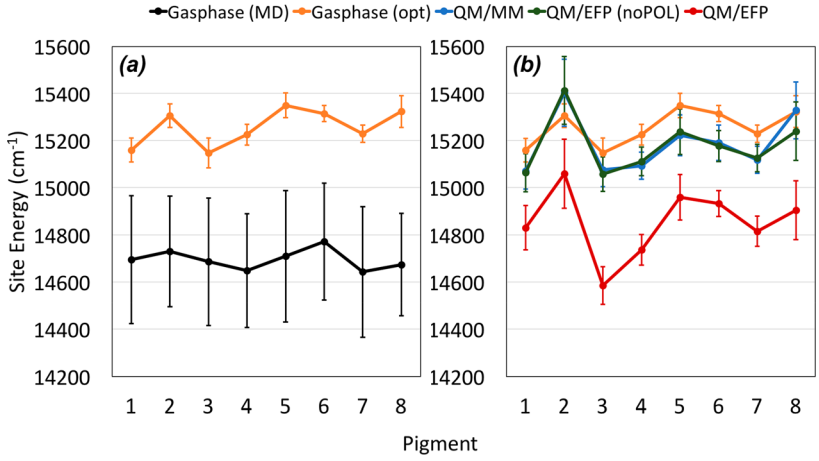

Figure 2. BChl *a* site energies averaged over 100 structures with standard deviations shown as vertical error bars. (a) Gas-phase (without protein environment) site energies computed for structures directly extracted from MD snapshots (black) and after QM/MM geometry optimizations (orange). (b) Gas phase (orange), QM/MM (blue), QM/EFP-noPOL (green), and QM/EFP (red) site energies computed for structures after QM/MM geometry optimizations.

in FMO, a number of different electronic Hamiltonians have been proposed,[6,8,10,12,14,18,19,23,25] most of which were obtained by a combination of structural data and fits to available experimental measurements. While the off-diagonal elements of a Hamiltonian represent electronic couplings between pigments and can be estimated using dipole−dipole approximation from available X-ray structures, the diagonal energies (individual transition energies) cannot be observed directly in experiment and are inferred from fits to spectroscopic data. This approach results in a significant ambiguity in determination of BChl *a* site energies and typically does not account for environment-driven variations in transition dipole moments of individual pigments and interpigment couplings. While molecular modeling based on structural data could provide unambiguous assignment of excitonic interactions and energy flow in FMO, internal complexity of the system and necessity to sample protein degrees of freedom and accurately describe electronic structure and couplings between BChl pigments [illegible] interactions between pigments and the protein environment makes this task challenging[24,26,27,29,35,42−44]

In this contribution, we report a multiscale first-principles modeling that accurately reproduces the absorption and circular dichroism (CD) spectra of the FMO complex based solely on its X-ray structure and uses no other input from experiments. We show that a quantum mechanical description of internal structures of BChl *a* pigments and embedding of pigments in a polarizable protein environment are the leading factors that provide excitonic structure consistent with experimental absorption and CD spectra. The developed protocol can be readily applied to other pigment−protein complexes with computational time scaling linearly with the number of antenna pigments.

The computational protocol, described in detail in the Supporting Information, consisted of three main steps. First, the structure of the FMO trimeric complex from *Chlorobaculum tepidum*, formerly known as *Chlorobium tepidum* (PDB ID: 3ENI), was protonated, immersed in water solvent, and equilibrated in a series of molecular dynamics (MD) simulations at ambient conditions with Amber03 classical force field. 100 configurations were extracted from the last 30 ns of the equilibrated MD trajectory, shown in Figure S1. Second, constrained quantum mechanics/molecular mechanics (QM/MM) geometry optimizations, with QM regions containing one BChl *a* pigment and few strongly interacting amino acids (AA) including the Mg-coordinating AA, were performed for each BChl *a* at each of the 100 selected configurations. Only the QM regions described with PBE0/6-

https://dx.doi.org/10.1021/acs.jpclett.9b03486
J. Phys. Chem. Lett. 2020, 11, 1636−1643

31G(d) and shown in Figure S2 of the Supporting Information were subject to geometry optimizations, thus removing inaccuracies caused by a classical force field description of the chromophore pocket. Finally, excited state calculations were performed at each structure with electrostatic embedding QM/MM and polarizable embedding QM/effective fragment potential (EFP) models. The extent of the quantum and classical regions for each BChl *a* is outlined in the Supporting Information (Figures S5 and S6); time-dependent density functional theory (TD-DFT) PBE0/6-31G(d) was used to describe electronic excitations. These calculations produced excitation site energies and transition charges for each BChl *a*; the latter were used to compute electronic couplings between pigments.

In the described computational procedure, two steps critically affect the quality of results, as we demonstrate below. These are (i) QM/MM geometry optimizations with sufficiently large QM regions and (ii) excited state calculations in a polarizable protein environment. As shown in Figure 2a, the electronic excitation energies of BChl *a* pigments (without inclusion of protein environment, aka "gas phase" site energies) with structures extracted directly from the MD trajectory snapshots are essentially indistinguishable between each other due to large fluctuations of BChl *a* internal structures during molecular dynamics and general limitations of the classical force field. On the other hand, gas-phase site energies computed at the QM/MM optimized structures fluctuate much less, such that energy differences between different sites become more pronounced. The differences in gas-phase site energies originate in geometrical constraints imposed by the protein scaffold on each BChl *a* pigment. Comparison of site energies computed at the MM-optimized and QM/MM optimized structures, shown in Figure S7, further demonstrates importance of correcting the BChl *a* structures at the QM level.

We also found that inclusion of several neighboring AAs in the QM regions significantly influenced the BChl *a* internal structures during the QM/MM geometry optimizations. The guideline for selecting these "critical" AAs came from considering effects of individual AAs on BChl *a* excitation energies, i.e, solvatochromic shifts due to individual neighboring AAs. Details of that procedure are discussed in the Supporting Information.

The second critical step in our computational protocol is employing polarizable QM/EFP model[45−51] for describing excitation energies of BChl *a* chromophores. The EFP method is a model potential providing a rigorous description of intermolecular interactions from first principles.[49,52−59] The EFP method treats a molecular system as a collection of rigid EFP fragments, interactions among which are described as a sum of Coulomb, polarization, dispersion, and exchange-repulsion terms. QM/EFP model, i.e. coupling of EFP subsystem to an *ab initio* region, can be classified as a polarizable embedding QM/MM approach in which effective fragments interact with the QM region via electrostatic and polarization one-electron operators.[47,51,52,60] Therefore, charge distribution on EFP fragments is able to respond self-consistently to electron density fluctuations of the QM region.[47,48] Electrostatic potential of EFP fragments is modeled using multipoles up to octupoles centered at atoms and bond-midpoints; polarization potential is modeled using induced dipoles created as a response of distributed anisotropic polarizabilities to the electric field due to surrounding fragments and QM region. Distributed multipoles and polarizabilities are precomputed for each unique fragment and stored as fragment parameters. A peptide chain is split into individual AA fragments along C−Cα bonds, as described in ref 50 and the Supporting Information.

To demonstrate the importance of polarizable embedding in description of excitation energies in the FMO complex, we compared the site energies (averaged over 100 snapshots) computed with electrostatic embedding models QM/MM and QM/EFP-noPOL and with polarizable embedding QM/EFP (see Figure 2b). Partial charges (Amber03, the same as in classical MD simulations) were used to represent the environment in QM/MM model, while distributed multipoles up to octupoles centered on atoms and bond midpoints were used in QM/EFP-noPOL model. QM/EFP utilizes both distributed multipoles and polarizabilities to account for self-consistent polarization of the QM region and its environment. As Figure 2b demonstrates, the QM/EFP-noPOL and QM/MM schemes produce similar average site energies implying that the inclusion of higher electrostatic multipoles in the description of electronic densities of AAs does not contribute significantly to solvatochromic shifts of BChl *a* pigments in the FMO complex. Noteworthy, both electrostatic embedding models do not differentiate well between different sites, producing similar solvatochromic shifts of 70−130 cm^{-1} for sites #1, #3, #4, #5, #6, and #7 (110−130 cm^{-1} shifts for sites #4, #5, #6, #7). In contrast to the electrostatic embedding models, the polarizable embedding QM/EFP results in distinct site energies and dramatically stabilizes excitation energy of site #3, which has been proposed to be an exit site of the FMO complex.[5,6,8,15,16,19,23,25]

Fluctuations of the QM/EFP site energies, originating in thermal motion of a protein scaffold captured by sampling of 100 protein structures, are visualized in Figure 3. Figure 3 also compares the average values of the QM/EFP site energies (shown with black vertical lines) with the excitation energies utilized in empirical Hamiltonians by Kell and Brixner (shown with blue and red arrows, respectively).[8,25] For an easier comparison with empirical Hamiltonians and experimental spectra, QM/EFP site energies are shifted by −2430 cm^{-1}, and QM/MM and QM/EFP-noPOL site energies are shifted by −2800 cm^{-1}. A mismatch between absolute values of experimental and computed excitation energies of BChls originates in well-known intrinsic inaccuracies of a chosen level of theory (PBE0 functional in 6-31G(d) basis set).[61,62] However, it is expected that the chosen level of theory reasonably describes a potential energy surface of the excited state (i.e., relative energy changes due to vibrational motion of a chromophore), and relative energy changes due to interaction of the excited state with the protein environment. It is these relative energy changes (due to slight geometrical distortions and interactions with the heterogeneous protein environment) that determine energetic order of site energies and shapes of the absorption and CD spectra.

As seen in Figure 3, there is a remarkable agreement between the average site energies from the QM/EFP model and Kell's and Brixner's Hamiltonians for the four lowest sites #1, #3, #4, and #7, while the energies of higher-energy sites deviate from each other. The deviations between empirical model Hamiltonians for high-energy sites are not surprising as it is harder to unambiguously deduce these energies from experiment due to short lifetimes and broader spectral bandwidth of high-energy states. On the other hand, the

https://dx.doi.org/10.1021/acs.jpclett.9b03486
J. Phys. Chem. Lett. 2020, 11, 1636−1643

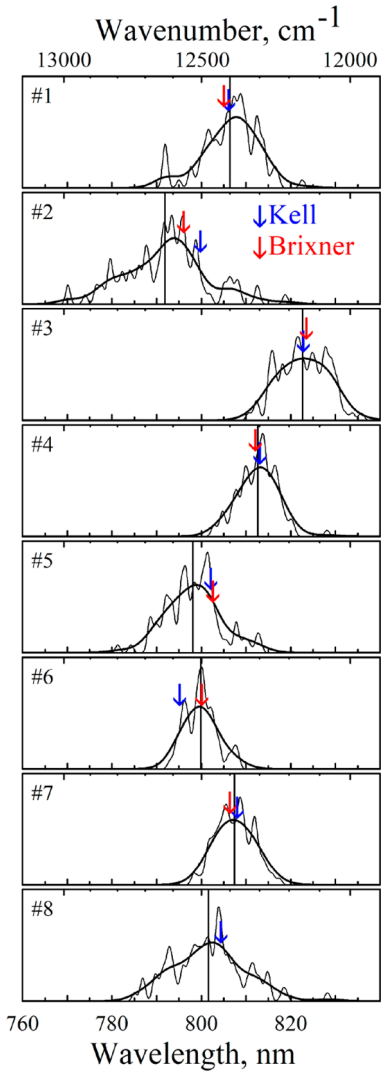

Figure 3. QM/EFP site energy fluctuations and comparison to model Hamiltonians by Kell[25] and Brixner.[8] QM/EFP excitation energies are shifted by −2430 cm^{-1} to match experimental absorption and CD spectra. Note that the Brixner Hamiltonian contains only seven pigments. QM/EFP site energy stick spectra of 100 snapshots of MD trajectory are broadened by Gaussians with fwhm of 20 (thinner black lines) and 100 cm^{-1} (thicker black lines). Average QM/EFP site energies are shown with black vertical lines; the site energies from Kell and Brixner empirical Hamiltonians are shown with blue and red arrows, respectively.

accuracy of the QM/EFP site energies is expected to be similar for all sites.

As follows from Figure 3, widths of energy distributions of sites #3, #4, #6, and #7 are comparable to each other. In general, bacteriochlorin heads of these sites have at least one H-bond with neighboring AAs in addition to coordination with N atoms of histidine (HIS) residues (see Figure S2 in the Supporting Information). On the contrary, sites #1, #5 and #8 do not have H-bonds to nearby AAs and are somewhat weaker bound to the protein scaffold. As a consequence, the excitation energy distribution of site #5 is wider than that of BChls that are H-bonded to a protein. Additionally, as site #8 is not fully embedded in a protein envelope, its motion is even less constrained, resulting in a significantly larger spread of excitation energies. In the case of site #2 that also shows a very large spread of energies, Mg is coordinated by a water molecule that moves freely in MD simulations such that BChl *a* #2 is found four-coordinated in about half of the snapshots. Additionally, several other water molecules that are present in a cavity near the BChl *a* #2 headgroup change their positions and H-bonding patterns during MD simulations and produce significant fluctuations to the site energy. Hence, we conclude that the width of the site energy distribution is largely governed by the effective H-bonding of BChl *a* heads with the protein scaffold as well as fluctuations of Mg-coordinating residues.

As a side note, analysis of excitation energies computed at 100 protein structures does not show any statistically significant correlation in fluctuations of site energies of different pigments, which agrees with previous discussion of this subject in literature.[15,29]

Electronic couplings were computed using transition charges TrEsp of each pigment obtained by a fit to a transition density with a constraint preserving the value of the transition dipole moment (TDM). Further, for computing electronic couplings, transition dipoles and corresponding transition charges were scaled to match (on average) experimental TDM of BChl *a*, as explained in detail in the Supporting Information. No additional environment-induced screenings were utilized in coupling calculations. Influence of polarizable environment on the electronic couplings in photosynthetic complexes was explored previously and found to be nonnegligible;[42,63,64] however, we leave a detailed analysis of these effects to future work.

Combining site energies with electronic couplings between different pairs of BChls, computed using transition charges TrEsp as explained in detail in the Supporting Information,

Average Hamiltonian

QM/EFP	1	2	3	4	5	6	7	8
1	14830.4	-113.4	5.3	-6.5	6.4	-8.9	-2.7	24.0
2	-113.4	15058.8	36.8	9.5	1.6	11.7	6.9	5.7
3	5.3	36.8	14585.3	-52.0	-2.0	-10.1	7.2	1.4
4	-6.5	9.5	-52.0	14736.3	-84.0	-19.3	-54.3	-2.0
5	6.4	1.6	-2.0	-84.0	14959.2	51.2	5.0	4.4
6	-8.9	11.7	-10.1	-19.3	51.2	14932.0	26.7	-11.2
7	-2.7	6.9	7.2	-54.3	5.0	26.7	14815.3	-14.1
8	24.0	5.7	1.4	-2.0	4.4	-11.2	-14.1	14904.9

Standard Deviation

QM/EFP	1	2	3	4	5	6	7	8
1	94.3	6.4	0.5	0.5	0.6	3.7	1.4	4.5
2	6.4	146.0	1.9	0.8	0.8	1.3	2.0	1.5
3	0.5	1.9	79.2	7.4	1.2	0.4	5.0	0.4
4	0.5	0.8	7.4	64.8	6.5	1.3	6.6	0.2
5	0.6	0.8	1.2	6.5	95.4	7.4	3.0	0.3
6	3.7	1.3	0.4	1.3	7.4	54.7	4.3	1.4
7	1.4	2.0	5.0	6.6	3.0	4.3	63.3	0.8
8	4.5	1.5	0.4	0.2	0.3	1.4	0.8	123.9

Figure 4. Averaged QM/EFP Hamiltonian and standard deviations of all matrix elements. All values are in cm^{-1}. The eighth pigment is BChl *a* #8′ as shown in Figure 1.

https://dx.doi.org/10.1021/acs.jpclett.9b03486
J. Phys. Chem. Lett. 2020, 11, 1636−1643

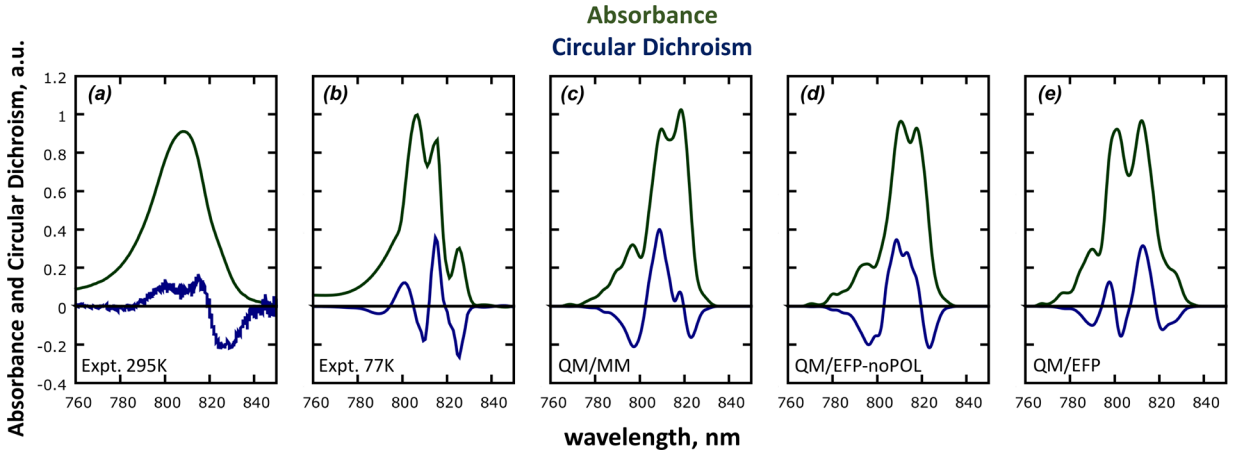

Figure 5. Absorption (green) and CD (blue) spectra of the FMO complex. Experimental spectra measured at 295 K (a) and 77 K (b) and computed spectra using QM/MM (c), QM/EFP-noPOL (d), and QM/EFP (e) models. Computed spectra are obtained by combining spectra of individual snapshots with a proportion of 45% of 7-site Hamiltonians and 55% of 8-site Hamiltonians. For a comparison with experimental spectra, QM/MM and QM/EFP-noPOL spectra are shifted by −2800 cm^{-1}, and QM/EFP spectra are shifted by −2430 cm^{-1}.

results in an electronic Hamiltonian that determines excitonic interactions in the FMO complex. The thermal motion of the protein produces fluctuations both of site energies and electronic couplings, such that each structural snapshot produces a unique Hamiltonian. Figure 4 provides an averaged QM/EFP Hamiltonian in which each matrix element is computed as an average of the corresponding matrix elements from 100 structures. Standard deviations of all Hamiltonian matrix elements are also shown in Figure 4. Analogous average QM/MM and QM/EFP-noPOL Hamiltonians are reported in Figure S9 of the Supporting Information. Note that these Hamiltonians include BChl *a* #8′ that is the closest to BChl *a* #1 (see Figure 1). While BChl *a* #8′ formally belongs to a different protein subunit, it interacts stronger with the pigments in this subunit than BChl *a* #8 that is positioned further away and has negligible interactions with pigments of the same unit. Inspection of the average Hamiltonian in Figure 4 shows that the couplings are the strongest between neighboring pigments, i.e. in pairs #1−2, #2−3, etc., which agrees with empirical Hamiltonians. Additionally, central BChl *a* #7 interacts strongly with site #4. Significant fluctuations in couplings are observed in pairs #5−6, #3−4, and #3−7.

Diagonalization of the electronic Hamiltonian produces excitonic states that are visualized and analyzed in Figure S11 of the Supporting Information. Overall, an excitonic map of a 7-site model (when BChl *a* #8′ is excluded from the Hamiltonian) is in an excellent agreement with that from Brixner's Hamiltonian,[8] while the 8-site model differs from Kell's Hamiltonian[25] in the relative order of pairs of excitons 5 and 6, and 7 and 8.

The excitonic Hamiltonian can be utilized to model absorption and CD spectra. Detailed comparison of spectra built off on the average electronic Hamiltonian and by averaging the spectra of different structural snapshots, as well as comparisons between transition charges and point dipole approximation models, is provided in the Supporting Information (Figures S12−S15). Here, we concentrate on comparing the absorption and CD spectra computed with the embedding models QM/MM, QM/EFP-noPOL, and QM/EFP. All spectra are computed as averages of spectra of individual structural snapshots, i.e. thermal motion of the protein is directly accounted for. These data are presented in Figure 5, together with experimental absorption and CD spectra measured at 295 and 77 K, as further described in the Supporting Information.

It is known from experimental studies[65] that BChl *a* #8 is only weakly bound in the FMO protein and an occupancy of site #8 depends on a protein preparation procedure. It is estimated that in the procedure utilized in samples that were used for measuring the spectra shown in Figures 5a and 5b, BChla *a* #8 is present in ∼55% of cases.[17,28] Thus, we mimicked a partial occupancy of site #8 by combining spectra of individual snapshots with a proportion of 45% of 7-site Hamiltonians and 55% of 8-site Hamiltonians.

Analyzing Figure 5, it is noteworthy that the quality of the QM/MM, QM/EFP-noPOL, and QM/EFP models cannot be deduced from comparing absorption spectra alone, as all three models produce two intense central peaks and red- and blue-side shoulders. However, the QM/EFP absorption spectrum appears to be somewhat more structured with a more pronounced red-side shoulder that corresponds to the absorption of the lowest energy excitonic state. CD spectra provide a more stringent test for the model accuracy, as the signal from different excitonic transitions can have both positive and negative signs. Out of the three computational models, only QM/EFP manages to reproduce characteristic (starting from the red side) down−up−down−up−down sequence of peaks observed both in room-temperature and low-temperature CD experiments, while the QM/MM and QM/EFP-noPOL models fail to reproduce a qualitative shape of the experimental CD spectra. A decomposition of the absorption and CD spectra into contributions of individual excitonic states is provided in the Supporting Information (Figures S12 and S13), from which it follows that the first (right-most, negative) and second (positive) peaks in CD are produced by the lowest energy excitons 1 and 2, while exciton 4 determines the third (negative) peak of CD. Interestingly, exciton 3 has opposite (positive or negative) CD signals in 7-site and 8-site models, due to the contribution of BChl *a* #8′. Overall, we conclude that only the polarizable QM/EFP model faithfully captures excitonic interactions in FMO and is capable of reproducing quantitatively both absorption and CD spectra.

We note in passing that the spectra modeled using electronic couplings computed with transition charges and point dipole

https://dx.doi.org/10.1021/acs.jpclett.9b03486
J. Phys. Chem. Lett. 2020, 11, 1636−1643

approximation are qualitatively similar, with the transition charge model producing a better-resolved lowest-energy (first exciton) shoulder in the absorption spectrum and a better-resolved middle region (795−805 nm) of the CD spectrum. Detailed comparisons of transition charges and point dipole approximation models are provided in the Supporting Information (Figures S9, S11, and S15).

To summarize, we developed a multiscale modeling strategy for describing excitonic properties of pigment−protein complexes. The modeling is based solely on the X-ray structure of the protein complex and does not use other input from experiments. The main steps of the modeling procedure include classical MD simulations, followed by partial correction of pigment structures by constrained QM/MM geometry optimizations. Then, the excited state calculations of electronic states and transition charges of chromophores are conducted with TD-DFT PBE0/6-31G(d) in polarizable embedding in which the protein is modeled with the effective fragment potentials. This computational protocol was successfully applied to model the excitonic properties of the Fenna−Matthews−Olson photosynthetic complex and resulted in the electronic Hamiltonian that is in an excellent quantitative agreement with previously proposed empirical Hamiltonians. The theory reproduces all major features of absorption and CD spectra of the FMO protein complex. We demonstrate that such an agreement between modeling and experiment becomes possible due to (i) utilizing accurate structures of photosynthetic pigments for computing excitation energies and (ii) representing the protein environment with a polarizable model. Successful first-principles-based modeling of the FMO complex opens exciting avenues for predictive modeling of other wild-type and mutated photosynthetic pigment−protein complexes that will provide mechanistic understanding of interactions in these complex systems.

■ ASSOCIATED CONTENT

Supporting Information

The Supporting Information is available free of charge at https://pubs.acs.org/doi/10.1021/acs.jpclett.9b03486.

Description of experimental methods and computational details (PDF)

■ AUTHOR INFORMATION

Corresponding Author

Lyudmila V. Slipchenko − *Department of Chemistry, Purdue University, West Lafayette, Indiana 47907, United States;* orcid.org/0000-0002-0445-2990; Email: lslipchenko@purdue.edu

Authors

Yongbin Kim − *Department of Chemistry, Purdue University, West Lafayette, Indiana 47907, United States*

Dmitry Morozov − *Nanoscience Center and Department of Chemistry, University of Jyväskylä, Jyväskylä 40014, Finland;* orcid.org/0000-0001-9524-948X

Sergei Savikhin − *Department of Physics and Astronomy, Purdue University, West Lafayette, Indiana 47907, United States*

Complete contact information is available at: https://pubs.acs.org/10.1021/acs.jpclett.9b03486

Notes

The authors declare no competing financial interest.

■ ACKNOWLEDGMENTS

The authors thank Prof. Gerrit Groenhof for sharing topology of BChl force fields. Y.K. and L.V.S. gratefully acknowledge support from the National Science Foundation (grant CHE-1800505). S.S., V.S., and L.V.S. acknowledge support from the Department of Energy, Office of Basic Energy Sciences (grant DE-SC0018239). D.M. acknowledges support from the Academy of Finland (grant 285481) and also thanks the CSC-IT Center for Science in Espoo, Finland, for providing computational resources. This research was also supported in part through computational resources provided by Information Technology at Purdue, West Lafayette, Indiana.

■ REFERENCES

(1) Orf, G. S.; Blankenship, R. E. Chlorosome antenna complexes from green photosynthetic bacteria. *Photosynth. Res.* **2013**, *116* (2), 315−331.

(2) Savikhin, S.; Struve, W. S. Ultrafast energy transfer in FMO trimers from the green bacterium Chlorobium tepidum. *Biochemistry* **1994**, *33*, 11200−11208.

(3) Savikhin, S.; Struve, W. S. Low-temperature energy transfer in FMO trimers from the green photosynthetic bacterium Chlorobium tepidum. *Photosynth. Res.* **1996**, *48*, 271−276.

(4) Buck, D. R.; Savikhin, S.; Struve, W. S. Ultrafast absorption difference spectra of the FMO protein at 19 K: Experiment and simulations. *Biophys. J.* **1997**, *72*, 24−36.

(5) Louwe, R. J. W.; Vrieze, J.; Hoff, A. J.; Aartsma, T. J. Toward an integral interpretation of the optical steady-state spectra of the FMO-complex of Prosthecochloris aestuarii. 2. Exciton simulations. *J. Phys. Chem. B* **1997**, *101* (51), 11280−11287.

(6) Vulto, S. I. E.; de Baat, M. A.; Louwe, R. J. W.; Permentier, H. P.; Neef, T.; Miller, M.; van Amerongen, H.; Aartsma, T. J. Exciton simulations of optical spectra of the FMO complex from the green sulfur bacterium Chlorobium tepidum at 6 K. *J. Phys. Chem. B* **1998**, *102* (47), 9577−9582.

(7) Vulto, S. I. E.; de Baat, M. A.; Neerken, S.; Nowak, F. R.; van Amerongen, H.; Amesz, J.; Aartsma, T. J. Excited state dynamics in FMO antenna complexes from photosynthetic green sulfur bacteria: a kinetic model. *J. Phys. Chem. B* **1999**, *103* (38), 8153−8161.

(8) Brixner, T.; Stenger, J.; Vaswani, H. M.; Cho, M.; Blankenship, R. E.; Fleming, G. R. Two-dimensional spectroscopy of electronic couplings in photosynthesis. *Nature* **2005**, *434* (7033), 625−628.

(9) Olson, J. The FMO protein. In *Discoveries in Photosynthesis*; Govindjee, Beatty, J. T., Gest, H., Allen, J., Eds.; Springer Netherlands: 2005; Vol. *20*, pp 421−427.

(10) Adolphs, J.; Muh, F.; Madjet, M. E. A.; Renger, T. Calculation of pigment transition energies in the FMO protein. *Photosynth. Res.* **2008**, *95* (2−3), 197−209.

(11) Tronrud, D. E.; Wen, J. Z.; Gay, L.; Blankenship, R. E. The structural basis for the difference in absorbance spectra for the FMO antenna protein from various green sulfur bacteria. *Photosynth. Res.* **2009**, *100* (2), 79−87.

(12) Milder, M. T. W.; Bruggemann, B.; van Grondelle, R.; Herek, J. L. Revisiting the optical properties of the FMO protein. *Photosynth. Res.* **2010**, *104* (2−3), 257−274.

(13) Moix, J.; Wu, J.; Huo, P.; Coker, D.; Cao, J. Efficient Energy Transfer in Light-Harvesting Systems, III: The Influence of the Eighth

Bacteriochlorophyll on the Dynamics and Efficiency in FMO. *J. Phys. Chem. Lett.* **2011**, *2* (24), 3045−3052.
(14) Olbrich, C.; Jansen, T. L. C.; Liebers, J.; Aghtar, M.; Strumpfer, J.; Schulten, K.; Knoester, J.; Kleinekathofer, U. From Atomistic Modeling to Excitation Transfer and Two-Dimensional Spectra of the FMO Light-Harvesting Complex. *J. Phys. Chem. B* **2011**, *115* (26), 8609−8621.
(15) Olbrich, C.; Strumpfer, J.; Schulten, K.; Kleinekathofer, U. Quest for Spatially Correlated Fluctuations in the FMO Light-Harvesting Complex. *J. Phys. Chem. B* **2011**, *115* (4), 758−764.
(16) Schmidt am Busch, M.; Müh, F.; El-Amine Madjet, M.; Renger, T. The Eighth Bacteriochlorophyll Completes the Excitation Energy Funnel in the FMO Protein. *J. Phys. Chem. Lett.* **2011**, *2* (2), 93−98.
(17) Wen, J.; Zhang, H.; Gross, M. L.; Blankenship, R. E. Native Electrospray Mass Spectrometry Reveals the Nature and Stoichiometry of Pigments in the FMO Photosynthetic Antenna Protein. *Biochemistry* **2011**, *50* (17), 3502−3511.
(18) Fidler, A. F.; Caram, J. R.; Hayes, D.; Engel, G. S. Towards a coherent picture of excitonic coherence in the Fenna−Matthews−Olson complex. *J. Phys. B: At., Mol. Opt. Phys.* **2012**, *45* (15), 154013.
(19) Gao, J. K.; Shi, W. J.; Ye, J.; Wang, X. Q.; Hirao, H.; Zhao, Y. QM/MM Modeling of Environmental Effects on Electronic Transitions of the FMO Complex. *J. Phys. Chem. B* **2013**, *117* (13), 3488−3495.
(20) List, N. H.; Curutchet, C.; Knecht, S.; Mennucci, B.; Kongsted, J. Toward Reliable Prediction of the Energy Ladder in Multi-chromophoric Systems: A Benchmark Study on the FMO Light-Harvesting Complex. *J. Chem. Theory Comput.* **2013**, *9* (11), 4928−4938.
(21) Jurinovich, S.; Curutchet, C.; Mennucci, B. The Fenna−Matthews−Olson Protein Revisited: A Fully Polarizable (TD)DFT/MM Description. *ChemPhysChem* **2014**, *15* (15), 3194−3204.
(22) Chandrasekaran, S.; Aghtar, M.; Valleau, S.; Aspuru-Guzik, A.; Kleinekathöfer, U. Influence of Force Fields and Quantum Chemistry Approach on Spectral Densities of BChl a in Solution and in FMO Proteins. *J. Phys. Chem. B* **2015**, *119* (31), 9995−10004.
(23) Jia, X. Y.; Mei, Y.; Zhang, J. Z. H.; Mo, Y. Hybrid QM/MM study of FMO complex with polarized protein-specific charge. *Sci. Rep.* **2015**, *5*, 17096.
(24) Higashi, M.; Saito, S. Quantitative Evaluation of Site Energies and Their Fluctuations of Pigments in the Fenna−Matthews−Olson Complex with an Efficient Method for Generating a Potential Energy Surface. *J. Chem. Theory Comput.* **2016**, *12* (8), 4128−4137.
(25) Kell, A.; Blankenship, R. E.; Jankowiak, R. Effect of Spectral Density Shapes on the Excitonic Structure and Dynamics of the Fenna−Matthews−Olson Trimer from Chlorobaculum tepidum. *J. Phys. Chem. A* **2016**, *120* (31), 6146−6154.
(26) Schulze, J.; Shibl, M. F.; Al-Marri, M. J.; Kühn, O. Multi-layer multi-configuration time-dependent Hartree (ML-MCTDH) approach to the correlated exciton-vibrational dynamics in the FMO complex. *J. Chem. Phys.* **2016**, *144* (18), 185101.
(27) Padula, D.; Lee, M. H.; Claridge, K.; Troisi, A. Chromophore-Dependent Intramolecular Exciton−Vibrational Coupling in the FMO Complex: Quantification and Importance for Exciton Dynamics. *J. Phys. Chem. B* **2017**, *121* (43), 10026−10035.
(28) Saer, R. G.; Stadnytskyi, V.; Magdaong, N. C.; Goodson, C.; Savikhin, S.; Blankenship, R. E. Probing the excitonic landscape of the Chlorobaculum tepidum Fenna−Matthews−Olson (FMO) complex: a mutagenesis approach. *Biochim. Biophys. Acta, Bioenerg.* **2017**, *1858* (4), 288−296.
(29) Kim, C. W.; Choi, B.; Rhee, Y. M. Excited state energy fluctuations in the Fenna−Matthews−Olson complex from molecular dynamics simulation with interpolated chromophore potentials. *Phys. Chem. Chem. Phys.* **2018**, *20* (5), 3310−3319.
(30) Matthews, B. W.; Fenna, R. E.; Bolognesi, M. C.; Schmid, M. F.; Olson, J. M. Structure of a bacteriochlorophyll *a*-protein from the green photosynthetic bacterium *Prosthecochloris aestuarii*. *J. Mol. Biol.* **1979**, *131* (2), 259−285.
(31) Buck, D. R.; Savikhin, S.; Struve, W. S. Effect of diagonal energy disorder on circular dichroism spectra of Fenna−Matthews−Olson trimers. *J. Phys. Chem. B* **1997**, *101* (42), 8395−8397.
(32) Savikhin, S.; Buck, D. R.; Struve, W. S. Toward level-to-level energy transfers in photosynthesis: the Fenna−Matthews−Olson protein. *J. Phys. Chem. B* **1998**, *102*, 5556−5565.
(33) Savikhin, S.; Buck, D. R.; Struve, W. S. The Fenna−Matthews−Olson protein: a strongly coupled photosynthetic antenna. In *Resonance Energy Transfer*; Andrews, D. L., Demidov, A. A., Eds.; John Wiley & Sons: New York, 1999; pp 399−434.
(34) Kihara, S.; Hartzler, D.; Orf, G. S.; Blankenship, R. E.; Savikhin, S. The Fate of the Triplet Excitations in the Fenna−Matthews−Olson Complex and Stability of the Complex. *Biophys. J.* **2014**, *106* (2), 182a.
(35) Saito, S.; Higashi, M.; Fleming, G. R. Site-Dependent Fluctuations Optimize Electronic Energy Transfer in the Fenna−Matthews−Olson Protein. *J. Phys. Chem. B* **2019**, *123*, 9762.
(36) Khmelnitskiy, A.; Reinot, T.; Jankowiak, R. Impact of Single-Point Mutations on the Excitonic Structure and Dynamics in a Fenna−Matthews−Olson Complex. *J. Phys. Chem. Lett.* **2018**, *9* (12), 3378−3386.
(37) Fransted, K. A.; Caram, J. R.; Hayes, D.; Engel, G. S. Two-dimensional electronic spectroscopy of bacteriochlorophyll a in solution: Elucidating the coherence dynamics of the Fenna−Matthews−Olson complex using its chromophore as a control. *J. Chem. Phys.* **2012**, *137* (12), 125101.
(38) Savikhin, S.; Buck, D. R.; Struve, W. S. Oscillating anisotropies in a bacteriochlorophyll protein: evidence for quantum beating between exciton levels. *Chem. Phys.* **1997**, *223*, 303−312.
(39) Allodi, M. A.; Otto, J. P.; Sohail, S. H.; Saer, R. G.; Wood, R. E.; Rolczynski, B. S.; Massey, S. C.; Ting, P.-C.; Blankenship, R. E.; Engel, G. S. Redox Conditions Affect Ultrafast Exciton Transport in Photosynthetic Pigment−Protein Complexes. *J. Phys. Chem. Lett.* **2018**, *9* (1), 89−95.
(40) Fidler, A. F.; Caram, J. R.; Hayes, D.; Engel, G. S. Towards a coherent picture of excitonic coherence in the Fenna−Matthews−Olson complex. *J. Phys. B: At., Mol. Opt. Phys.* **2012**, *45* (15), 154013.
(41) Engel, G. S. Quantum coherence in photosynthesis. *Procedia Chem.* **2011**, *3* (1), 222−231.
(42) Curutchet, C.; Mennucci, B. Quantum Chemical Studies of Light Harvesting. *Chem. Rev. (Washington, DC, U. S.)* **2017**, *117* (2), 294−343.
(43) Groenhof, G.; Modi, V.; Morozov, D. Observe while it happens: catching photoactive proteins in the act with non-adiabatic molecular dynamics simulations. *Curr. Opin. Struct. Biol.* **2020**, *61*, 106−112.
(44) Kaliakin, D. S.; Nakata, H.; Kim, Y.; Chen, Q.; Fedorov, D. G.; Slipchenko, L. V. FMOxFMO: Elucidating Excitonic Interactions in the Fenna−Matthews−Olson Complex with the Fragment Molecular Orbital Method. *J. Chem. Theory Comput.* **2020**, DOI: 10.1021/acs.jctc.9b00621.
(45) Kosenkov, D.; Slipchenko, L. V. Solvent effects on the electronic transitions of p-nitroaniline: A QM/EFP study. *J. Phys. Chem. A* **2011**, *115* (4), 392−401.
(46) Ghosh, D.; Isayev, O.; Slipchenko, L. V.; Krylov, A. I. Effect of solvation on the vertical ionization energy of thymine: from microhydration to bulk. *J. Phys. Chem. A* **2011**, *115* (23), 6028−6038.
(47) Slipchenko, L. V. Solvation of the Excited States of Chromophores in Polarizable Environment: Orbital Relaxation versus Polarization. *J. Phys. Chem. A* **2010**, *114* (33), 8824−8830.
(48) DeFusco, A.; Minezawa, N.; Slipchenko, L. V.; Zahariev, F.; Gordon, M. S. Modeling Solvent Effects on Electronic Excited States. *J. Phys. Chem. Lett.* **2011**, *2* (17), 2184−2192.
(49) Gordon, M. S.; Smith, Q. A.; Xu, P.; Slipchenko, L. V. Accurate First Principles Model Potentials for Intermolecular Interactions. *Annu. Rev. Phys. Chem.* **2013**, *64*, 553−578.
(50) Gurunathan, P. K.; Acharya, A.; Ghosh, D.; Kosenkov, D.; Kaliman, I.; Shao, Y. H.; Krylov, A. I.; Slipchenko, L. V. Extension of

the Effective Fragment Potential Method to Macromolecules. *J. Phys. Chem. B* **2016**, *120* (27), 6562−6574.
(51) Slipchenko, L. V.; Gurunathan, P. K. Effective Fragment Potential Method: Past, Present, and Future. In *Fragmentation: Toward Accurate Calculations on Complex Molecular Systems*; Gordon, M. S., Ed.; Wiley: 2017; pp 183−208.
(52) Day, P. N.; Jensen, J. H.; Gordon, M. S.; Webb, S. P.; Stevens, W. J.; Krauss, M.; Garmer, D.; Basch, H.; Cohen, D. An effective fragment method for modeling solvent effects in quantum mechanical calculations. *J. Chem. Phys.* **1996**, *105* (5), 1968−1986.
(53) Gordon, M. S.; Freitag, M. A.; Bandyopadhyay, P.; Jensen, J. H.; Kairys, V.; Stevens, W. J. The effective fragment potential method: A QM-based MM approach to modeling environmental effects in chemistry. *J. Phys. Chem. A* **2001**, *105* (2), 293−307.
(54) Gordon, M. S.; Slipchenko, L.; Li, H.; Jensen, J. H. Chapter 10: The Effective Fragment Potential: A General Method for Predicting Intermolecular Interactions. In *Annual Reports in Computational Chemistry*; Spellmeyer, D. C., Wheeler, R., Eds.; Elsevier: 2007; Vol. 3, pp 177−193.
(55) Kaliman, I. A.; Slipchenko, L. V. LIBEFP: A new parallel implementation of the effective fragment potential method as a portable software library. *J. Comput. Chem.* **2013**, *34* (26), 2284−2292.
(56) Kaliman, I. A.; Slipchenko, L. V. Hybrid MPI/OpenMP Parallelization of the Effective Fragment Potential Method in the libefp Software Library. *J. Comput. Chem.* **2015**, *36* (2), 129−135.
(57) Ghosh, D.; Kosenkov, D.; Vanovschi, V.; Williams, C. F.; Herbert, J. M.; Gordon, M. S.; Schmidt, M. W.; Slipchenko, L. V.; Krylov, A. I. Noncovalent interactions in extended systems described by the effective fragment potential method: Theory and application to nucleobase oligomers. *J. Phys. Chem. A* **2010**, *114* (48), 12739−12754.
(58) Slipchenko, L. V. Effective Fragment Potential Method. In *Many-Body Effects and Electrostatics in Biomolecules*; Cui, Q., Meuwly, M., Ren, P., Eds.; CRC Press: 2016; pp 147−190.
(59) Gordon, M. S.; Fedorov, D. G.; Pruitt, S. R.; Slipchenko, L. V. Fragmentation methods: a route to accurate calculations on large systems. *Chem. Rev. (Washington, DC, U. S.)* **2012**, *112* (1), 632−672.
(60) Gordon, M. S.; Fedorov, D. G.; Pruitt, S. R.; Slipchenko, L. V. Fragmentation Methods: A Route to Accurate Calculations on Large Systems. *Chem. Rev. (Washington, DC, U. S.)* **2012**, *112* (1), 632−672.
(61) Sisto, A.; Glowacki, D. R.; Martinez, T. J. Ab Initio Nonadiabatic Dynamics of Multichromophore Complexes: A Scalable Graphical-Processing-Unit-Accelerated Exciton Framework. *Acc. Chem. Res.* **2014**, *47* (9), 2857−2866.
(62) Segatta, F.; Cupellini, L.; Garavelli, M.; Mennucci, B. Quantum Chemical Modeling of the Photoinduced Activity of Multichromophoric Biosystems. *Chem. Rev. (Washington, DC, U. S.)* **2019**, *119* (16), 9361−9380.
(63) Curutchet, C.; Kongsted, J.; Muñoz-Losa, A.; Hossein-Nejad, H.; Scholes, G. D.; Mennucci, B. Photosynthetic Light-Harvesting Is Tuned by the Heterogeneous Polarizable Environment of the Protein. *J. Am. Chem. Soc.* **2011**, *133* (9), 3078−3084.
(64) Aghtar, M.; Kleinekathöfer, U.; Curutchet, C.; Mennucci, B. Impact of Electronic Fluctuations and Their Description on the Exciton Dynamics in the Light-Harvesting Complex PE545. *J. Phys. Chem. B* **2017**, *121* (6), 1330−1339.
(65) Ben-Shem, A.; Frolow, F.; Nelson, N. Evolution of photosystem I − from symmetry through pseudosymmetry to asymmetry. *FEBS Lett.* **2004**, *564* (3), 274−280.

https://dx.doi.org/10.1021/acs.jpclett.9b03486
J. Phys. Chem. Lett. 2020, 11, 1636−1643